Effect of recrystallization on ion-irradiation hardening and microstructural changes in 15Cr-ODS steel

Yoosung Ha[1] and Akihiko Kimura[2]

[1]Graduate school of Energy Science, Kyoto University, Uji, Kyoto, Japan

[2]Institute of Advanced Energy, Kyoto University, Uji, Kyoto, Japan

Abstract

The effects of recrystallization on ion-irradiation hardening and microstructural changes were investigated for a 15Cr-ODS ferritic steel. Dual ion-irradiation experiments were performed at 470 °C using 6.4 MeV Fe^{3+} ions simultaneously with energy-degraded 1 MeV He^{+} ions. The displacement of damage at 600 nm depth from the specimen surface was 30 dpa. Nano-indentation test with Berkovich type indentation tip was measured by constant stiffness measurement (CSM) technique. Results from nano-indentation tests indicate irradiation hardening in ODS steels even at 470°C, while it wasn't observed in reduced activation ferritic steel. Recrystallized ODS steel shows a larger irradiation hardening, which is considered to be due to the reduction of grain boundaries and interfaces of matrix/oxide particles. In 20 % cold rolled ODS steel after recrystallization, both the hardening and bubble number density were lower than those of recrystallized ODS steel, suggesting that dislocations generated by cold rolling suppress bubble formation. Based on the estimation of irradiation hardening from TEM observation results, it is considered that the bubbles are not the main factor controlling ion-irradiation hardening.

Keywords: Dual ion irradiation, Irradiation hardening, Defect trapping and absorption

1. Introduction

Oxide dispersion strengthened (ODS) steels have been considered as one of candidate structural materials for fusion blankets because they show a high-strength at elevated temperatures and radiation tolerance [1, 2]. Both the high performances observed in ODS steels are due to not only oxide particles dispersed in high number density but also fine grains, which provide a large number of trapping sites for radiation defects and helium atoms at the interfaces of matrix/oxide particles and grain boundaries, and intensively suppress defect clustering to form large dislocation loops and helium bubbles [3].

Because of hot-extrusion and tubing processes of ODS steels, the grains are elongated to the direction of the hot extrusion and causes anisotropy in mechanical properties [4]. Therefore, recrystallization treatment is necessary to achieve enough ductility in the radial direction to prevent the ODS tubes from cracking during the tube production processes.

It is expected that in the recrystallized ODS steels the trapping sites for irradiation damage structures are significantly reduced because of the reduction of grain boundary area. In this research, the effect of recrystallization on ion-irradiation effects in 15Cr-ODS ferritic steels is investigated to clear the role of grain boundaries as well as oxide particles on the irradiation hardening and microstructural evolution.

2. Material and methods

The material used in this study is an ODS ferritic steel composed of Fe (bal.)-15Cr-2W-4Al-0.5Zr-0.33Y_2O_3. Three specimens with different final treatment conditions were prepared: 1) “as-received” specimens are those as received after heat treatment at 1150 °C for 1 hr. 2) “recrystallized” specimens are those annealed at 1350 °C for 1 hr. 3) “cold-rolled” specimens are those cold-rolled with 20 % thickness reduction ratio after the above recrystallization. Table 1 shows the characteristics of three specimens of the ODS steel with different final treatment conditions. The grain size is significantly larger and oxide particles are coarser in the recrystallized specimen than as-received one, which causes the reduction of Vickers hardness. The cold-rolling after the recrystallization resulted in an increase in Vickers hardness, which is due to work hardening.

All specimens were mechanically grinded with SiC emery papers and buff-polished with diamond pastes. Finally, electrolytic polishing was performed to remove the damaged surface layer resulting from mechanical polishing. A solution of 5 vol. % perchloric acid and 95 vol. % methanol was used for electrolytic polishing at 18 V for 2~3 seconds at -50 °C with addition of liquid nitrogen [3].

Ion-irradiation experiments were performed at 470 °C using dual-ion beam irradiation experimental test facility (DuET), which consisted of two Cockcroft-Walton type accelerators to simulate the irradiation condition of fusion reactor environment [5, 6]. Three specimens were simultaneously irradiated with 6.4 MeV Fe^{3+} ions at a nominal displacement rate of 4×10^{-4} dpa/s and 1.0 MeV He^{+} ions at a helium implantation rate of 15 appm He/dpa with an energy-degrader for homogenous implantation of He^{+} ions.

The depth profiles of displacement per atoms, dpa, and implanted He^{+} ions, appm, obtained by SRIM code calculations are shown in Fig. 1. The nominal dpa is designated as the displacement damage occurring at the depth of 600 nm from the irradiated surface [7-9], and in this study it was 30 dpa. The implanted helium range was between 200 and 1500 nm depth from the specimen surface.

Nano-indentation tests were carried out on the specimen surface of ion-irradiated specimens using G200 Nano Indenter (Agilent Technologies Inc.) with Berkovich type indentation tip, which has 65° between the indentation direction and indented surface. The constant stiffness measurement (CSM) technique was used to measure the depth profile of hardness [9]. The indentation hardness profiles were averaged for 20 measured profiles for each specimen.

Specimens for TEM observation were sampled by Focus Ion Beam (FIB) technique. After FIB sampling, the specimen was polished with a Nano-mill system (Model 1040, Fischione Instruments, Inc.), which removed the region damaged by FIB treatment. The microstructural changes by ion irradiation were examined by TEM (JEM-2010, JEOL Co.) with an acceleration voltage of 200 kV.

3. Results and Discussion

3.1. Irradiation hardening

Fig. 2 (a), (b) and (c) show the averaged depth profiles of twenty of indentation hardness measurements of (a) as-received, (b) recrystallized and (3) cold-rolled specimen before and after ion-irradiation. In general, the hardness decreases with increasing displacement, which is well known as indentation size effect (ISE) [10]. Irradiation hardening is observed in all the cases irrespective of final treatment conditions. Fig. 2 (d) is the dependence of irradiation hardening, $\Delta H = H_{IRR} - H_{UNIRR}$, on the indentation displacement for each specimen. The hardening shows a peak at around 250 nm in the case of recrystallized specimen.

It is of notice that in ODS steel, irradiation hardening is observed after the irradiation at

470 °C, while in the conventional (non-ODS) steels it was not observed when the irradiation temperature was higher than 420 °C [11-15] because of the mutual annihilation between interstitial type dislocation loops (I-loops) and vacancies decomposed from vacancy clusters. The irradiation hardening observed in the ODS steel is considered to be due to vacancy trapping effect in the steels where the interfaces of matrix/oxide particles play a role in trapping vacancies, consequently the mutual annihilation of I-loops and vacancies is suppressed even at 470 °C. In this experiment, the specimens were irradiated with dual ions including He^+, most of vacancies formed V-He pairs.

The irradiation hardening is largest in the recrystallized specimen, suggesting that the number density of I-loops, which is considered to be the main factor controlling irradiation hardening, is largest among three specimens. As shown in Table 1, recrystallization resulted in a significant reduction of both the area of grain boundaries and the matrix/particle interfaces. It is considered that grain boundaries absorb both interstitial atoms and vacancies, while the matrix/particle interfaces absorb only vacancies and/or V-He, so that free interstitial atoms increase to form a large number of I-loops. The dislocations generated by cold rolling play a role similar to grain boundaries in absorbing both interstitial atoms and vacancies, resulting in the rather remarkable reduction of irradiation hardening.

3.2. Microstructure observation

Fig. 3 shows the cross sectional views of each irradiated specimen observed by TEM with a diffraction of dislocation (top) and bubble (bottom) contrast. The SRIM calculation results of depth profile of dpa and He/dpa are overdrawn on the micrographs. A lot of dislocation loops and line dislocations were observed in the damaged area of all the specimens. Many bubbles are also observed in the irradiated area in both the recrystallized specimens but not in as-received specimen. The irradiated area can be distinguished with unirradiated one because the large dislocation loops and unfold dislocations are observed in the irradiated area, while only line shape dislocations (marked by black arrow) are pre-existing in the unirradiated area that is deeper than 2 μm.

Fig. 4 shows dislocation microstructure and He bubbles. Both the line dislocations and rather large dislocation loops are observed in all the specimens. Generally, the size of dislocation loop is increased with increasing irradiation temperature [16], and a part of line dislocations are those unfold dislocation loops induced by the irradiation. Although a number of fine black dots are observed some area, these are expected to be produced during FIB specimen preparation process, since these structures are also observed in the unirradiated area.

A number of helium bubbles are observed in recrystallized specimens. Many large bubbles are formed at the interfaces of matrix/oxide particles, indicating that V-He pairs are trapped at the interfaces to grow to large He bubbles. The number density of the bubbles is reduced in the cold rolled specimen after recrystallization. This is interpreted in terms of absorption of V-He pair at the pre-existed dislocations. Only a few bubbles are observed in as-received specimen. The grain boundaries also play a role as trapping sites for irradiation damage structures. In the case of recrystallized ODS steel, the grain size increased, which means grain boundary area as a trapping site is reduced. The total interface area of matrix/oxide particles is also decreased after recrystallization. The reduced trapping sites resulted in the formation of bubbles consisting of vacancies and helium atoms. Therefore, when grain boundaries are scarce, the vacancy clusters are easily formed in the grains.

3.3. Estimation of irradiation hardening

Irradiation hardening has been often shown by equation (1) that is the sum of hardenings by each radiation damage structures such as interstitial clusters, vacancy clusters and helium-vacancy clusters. According to the present TEM observation results, it is expected that the irradiation hardening of the ODS steel irradiated at 470 °C is due to dislocations including rather large dislocation loops, line shape dislocations and He bubbles. Since the dislocation loops can grow to large loops and to convert to unfold dislocations at 470 °C, it is expected that not small dislocation loops but line dislocations and large dislocation loops only contribute to the irradiation hardening. Thus, the hardening is expressed by the equation (2).

$$\Delta H_{total} = \Delta\sigma_{disl.line} + \Delta\sigma_{disl.loops} + \Delta\sigma_{bubbles} \quad (1)$$

$$\Delta\sigma_{disl.} = M\alpha\mu b(\sqrt{\rho} + \sqrt{N \cdot d}\,) \quad (2)$$

where $\Delta\sigma_{disl.}$ is the increase in the tensile yield stress, M is the Taylor factor (3.04), μ is the shear modulus (8.05×10^4 MPa [17]), b is the Burgers vector (0.286 nm), and ρ is dislocation density. N is the number density and d is the diameter of dislocation loops. α is strength factor ($0 < \alpha < 1$), indicating a measure of barrier against dislocation motion [18]. In this research, $\alpha = 0.212$ and 0.65 is used for line dislocations and dislocation loops, respectively. Helium bubbles may also contribute to the hardening by the equation (3).

$$\Delta\sigma_{bubble} = M\alpha\mu b\sqrt{N \cdot d} \quad (3)$$

where $\Delta\sigma_{bubbles}$ is the increase in the tensile yield stress, N is the number density and d is the diameter of bubbles. It is applicable to recrystallized and cold rolled ODS steels, in which bubbles were observed in irradiated area. The factor α for bubble strengthening is assumed to be 0, 0.1 and 0.2.

Fig. 5 shows the distributions of dislocation density and the number density of bubbles in the irradiated area estimated from TEM observation results of each specimen. Both distribution profiles are similar to the damage profile in Fig. 1, indicating that the damage peak is in the range between 1000 and 1500 nm. Bubble number density of cold rolled ODS steel is lower than that of recrystallized ODS steel in all areas**.** Numerical results of characteristic features of irradiation-induced microstructures in three specimens of the ODS steel with different final treatment conditions were summarized in Table 2.

The total hardening estimated from the data is shown in Table 3. Here, the tensile yield stress was converted into the hardness using a relationship, $\Delta\sigma$ (MPa) = 0.3ΔH (MPa) [19]. The hardening measured by nano-indentation tests at the displacement of 250 nm is compared with that estimated from Table 2. The hardness from indentation testing is affected by around 3~6 times area of indented depth [9, 20], the experimental hardening at 250 nm involved the hardness at 1500 nm. Regardless of α factor for bubbles, all results of estimated hardenings are higher than that of experiment hardening in recrystallized ODS steel. The estimated hardening only shows similar a tendency with experimental hardening in the cases of α=0 and 0.1. (Recrystallized>as-received>cold rolled). It is considered that the bubbles are not the main factor controlling ion-irradiation hardening.

Conclusions

The effect of recrystallization on the ion-irradiation hardening of 15Cr-ODS steels were investigated after simultaneous irradiation of Fe^{3+} and He^{+}. The irradiation performances after recrystallization and cold rolling are different with microstructural changes such as grain boundaries, oxide particles distributions and dislocations by pre-existing or generated by cold rolling. The obtained main results are as follows:

1) After the irradiation at 470 °C to 30 dpa with 450 appm of helium implantation, irradiation hardening is still observed in ODS steel, which is in contrast to that

conventional steels show no hardening after irradiation at temperatures above 420 °C. This is considered to be due to stabilization of dislocations by trapping vacancies of the interfaces of oxide particles and the matrix.

2) Recrystallization enhances irradiation hardening, because both grain boundaries and interfaces between matrix and oxide particles, which absorb radiation damages, are significantly reduced by the annealing.
3) Large bubbles are formed with high number density in the recrystallized ODS steel but not in the as-received ODS steel, which has a high number of trapping sites. The bubble density is lower in cold rolled ODS steel than that of recrystallized ODS steel, which is attributed to the suppression of bubble formation by the dislocations generated by cold rolling.
4) Based on the estimation of irradiation hardening from TEM observation results, it is considered that the bubbles are not the main factor controlling ion-irradiation hardening, although the largest hardening is observed for the specimen in which rather large bubbles were formed.

Acknowledgements

The authors would like to thank Professor Kondo and Mr. Hashitomi, Mr. Omura for support to irradiation experiments and TEM observations with DuET facility in IAE, Kyoto University.

Reference

[1] P. Yvon, F. Carré, J. Nucl. Mater., 385 (2009) 217-222

[2] A. Kimura, H. S. Cho, N. Toda, R. Kasada, K. Yutani, H. Kishimoto, N. Iwata, S. Ukai, M. Fujiwara, J. Nucl. Sci. and Tech., 44 (2007) 323-328

[3] H. Kishimoto, K. Yutani, R. Kasada, A. Kimura, Fusion Eng. Des., 81 (2006) 1045-1049

[4] J. Saito, T. Suda, S. Yamashita, S. Ohnuki, H. Takahashi, N. Akasaka, M. Nishida, S. Ukai, J. Nucl. Mater., 258-263 (1998) 1264-1268

[5] A.Kohyama, Y. Katoh, M. Ando, K. Jimbo, Fusion Eng. Des., 51-52 (2002) 789-795

[6] K. Yutani, H. Kishimoto, R. Kasada, A. Kimura, J. Nucl. Mater., 367-370 (2007) 423-427

[7] www.srim.org

[8] James F. Ziegler, M. D. Ziegler, J. P. Biersack, Nucl. Instr. Meth. Phys. Res. B, 268 (2010) 1818-1823

[9] K. Yabuuchi, R. Kasada, A. Kimura, J. Nucl. Mater. 442 (2013) S790-S795

[10] Y. Takayama, R. Kasada, Y. Sakamoto, K. Yabuuchi, A. Kimura, M. Ando, D. Hamaguchi, H. Tanigawa, J. Nucl. Mater. 442 (2013) S23-S27

[11] A. Kimura, R. Kasada, A. Kohyama, H. Tanigawa, T. Hirose, K. Shiba, S. Jitsukawa, S. Ohtsuka, S. Ukai, M.A. Sokolov, R.L. Klueh, T. Yamamoto, G.R. Odette, J. Nucl. Mater., 367-370 (2007) 60-67

[12] A.-A.F. Tavassoli, J. Nucl.Mater. 302 (2002) 73-88

[13] S. Jitsukawa, M. Tamura, B. van der schaaf, R. L. Klueh, A. Alamo, C. Petersen, M. Schirra, P. paetig, G. R. Odette, A. A. Tavassoli, K. Shiba, A. Kohyama, A. Kimura, J. Nucl. Mater. 307-311 (2002) 179-186

[14] R. L. Klueh, K. Shiba, M. A. Sokolov, J. Nucl. Mater. 377 (2008) 427-437

[15] N. Okubo, Y. Miwa, K. Kondo, Y. Kaji, J. Nucl. Mater. 386-388 (2009) 290-293

[16] M. Kiritani, N. Yoshida, H. Takata, Y. Maehara, J. Phys. Soc. Jpn. 38 (1975) 1677-1686

[17] G. Ghosh, G. B. Olson, Acta Mater. 50 (2002) 2655-2675

[18] L. I. Ivanov, Yu. M. Platov, Radiation Physics of Metals and Its Applications, (Cambridge International Science Publishing, 2004), p. 272

[19] J.T. Busby, M.C. Hash, G.S. Was, J. Nucl. Mater. 336 (2005) 267-278

[20] C. W. Shih, M. Yang, J. C. M. Li, J. Mater. Res., Vol. 6, 12 (1991) 2623-2628

Figure captions

Table 1 Microstructure characteristics of three types of an ODS steel with different final treatment conditions.

Table 2 Numerical results of characteristic features of irradiation-induced microstructures in three types of an ODS steel with different final treatment conditions.

Table 3 The estimated irradiation hardening and experimentally measured hardening at 250 nm of indentation depth.

Fig. 1 Depth profiles of the displacement damage and implanted ions obtained from SRIM calculations at the irradiation conditions; (a) iron ions and (b) helium ions

Fig. 2 Depth profiles of the nano-indentation hardness of (a) as-received, (b) recrystallized, (c) cold rolled ODS steel and (d) irradiation hardening that is the subtraction of the hardness before and after irradiation up to 30 dpa at 470 °C.

Fig. 3 TEM microstructures observed with a dislocation contrast (top) and void contrast (bottom) showing the depth profiles calculated by SRIM code for dual-ion irradiated (a) as-received, (b) recrystallized and (c) cold rolled ODS steel.

Fig. 4 More detailed TEM microstructures observed with a dislocation contrast (left) and void contrast (right).

Fig. 5 The distribution profiles of dislocation with <200> *g vector* (bottom) and bubble number density (top) after dual-ion irradiation.

Table 1 Microstructure characteristics of three types of an ODS steel with different final treatment conditions

Type	Hv (MPa)	Ave. grain diameter (μm)	Oxide particles		Dislocation density (m^{-2})
	NI-H (MPa) at 250nm		Ave. diameter (nm)	Number density (m^{-3})	
1) As-received	2,696 4,872	1.6	11	8.4×10^{21}	3.08×10^{14}
2) Recrystallized	2,176 3,903	230	23	1.9×10^{21}	3.52×10^{13}
3) Cold-rolled	2,871 4,977	-	-	-	3.79×10^{14}

Table 2 Numerical results of characteristic features of irradiation-induced microstructures in three types of an ODS steel with different final treatment conditions

Type		ΔNI-H (MPa) at 250nm	Bubbles at 1000 nm		Dislocation density (m^{-2}) at 1000 nm
			Ave. diameter (nm)	Number density (m^{-3})	
1)	As-received	811	-	-	5.28×10^{14}
2)	Recrystallized	1,079	27	1.15×10^{21}	5.05×10^{14}
3)	Cold-rolled	447	28	3.56×10^{20}	5.24×10^{14}

Fig. 1 Depth profiles of the displacement damage and implanted ions obtained from SRIM calculations at the irradiation conditions; (a) iron ions and (b) helium ions

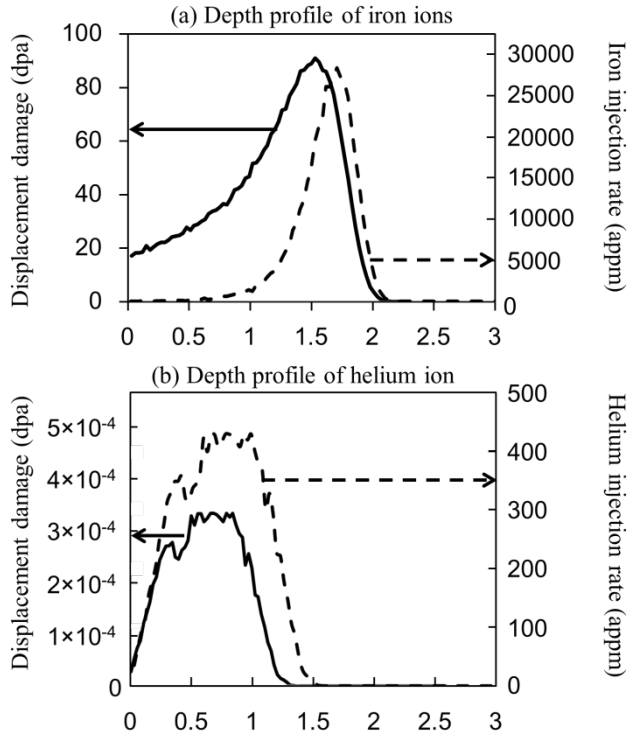

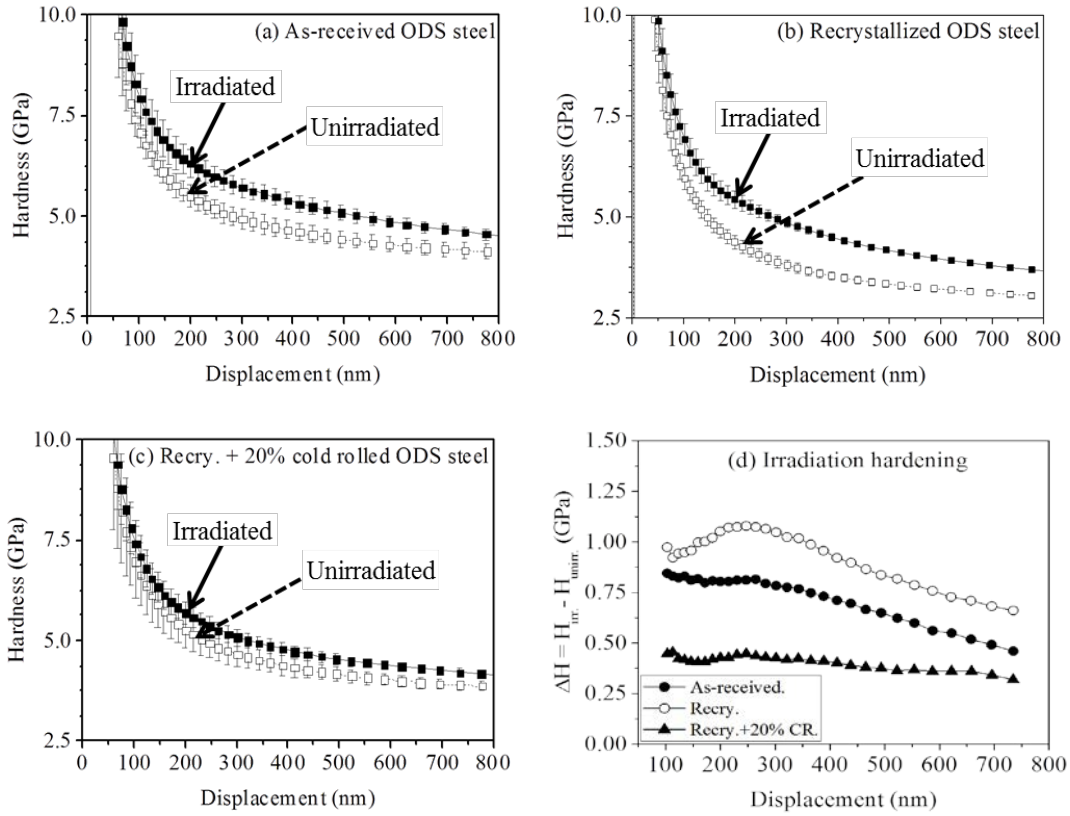

Fig. 2 Depth profiles of the nano-indentation hardness of (a) as-received, (b) recrystallized, (c) cold rolled ODS steel and (d) irradiation hardening that is the subtraction of the hardness before and after irradiation up to 30 dpa at 470 °C

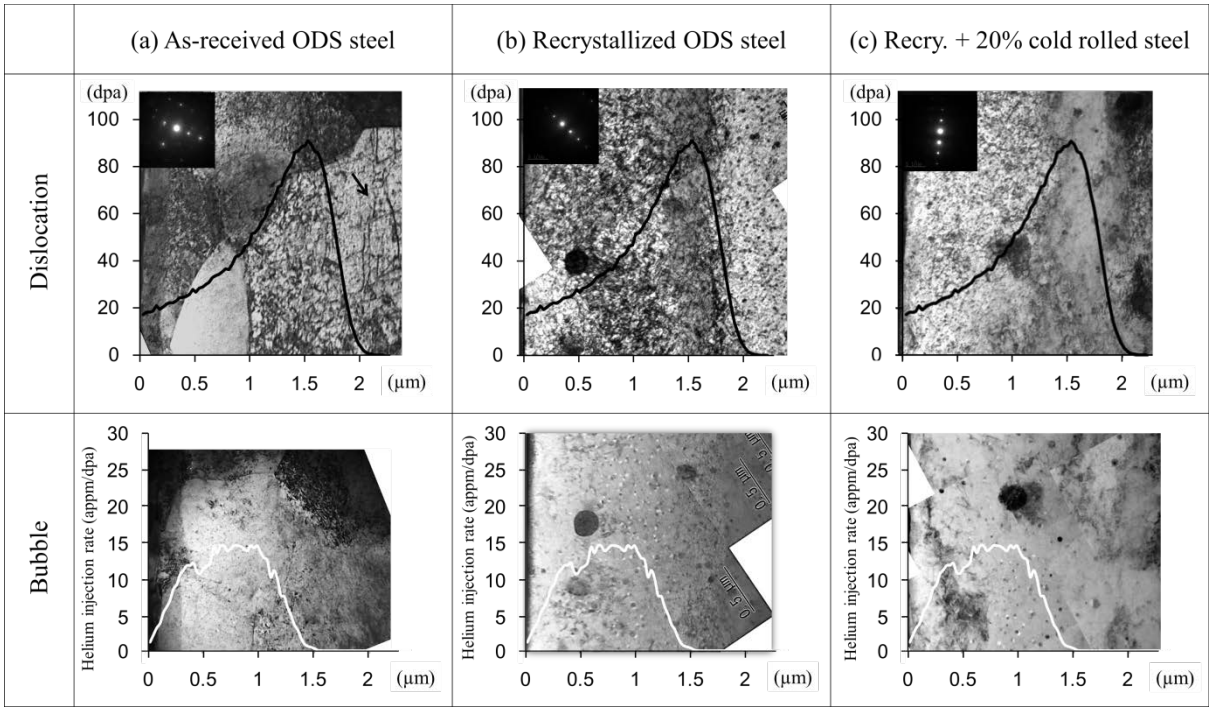

Fig. 3 TEM microstructures observed with a dislocation contrast (top) and void contrast (bottom) showing the depth profiles calculated by SRIM code for dual-ion irradiated (a) as-received, (b) recrystallized and (c) cold rolled ODS steel

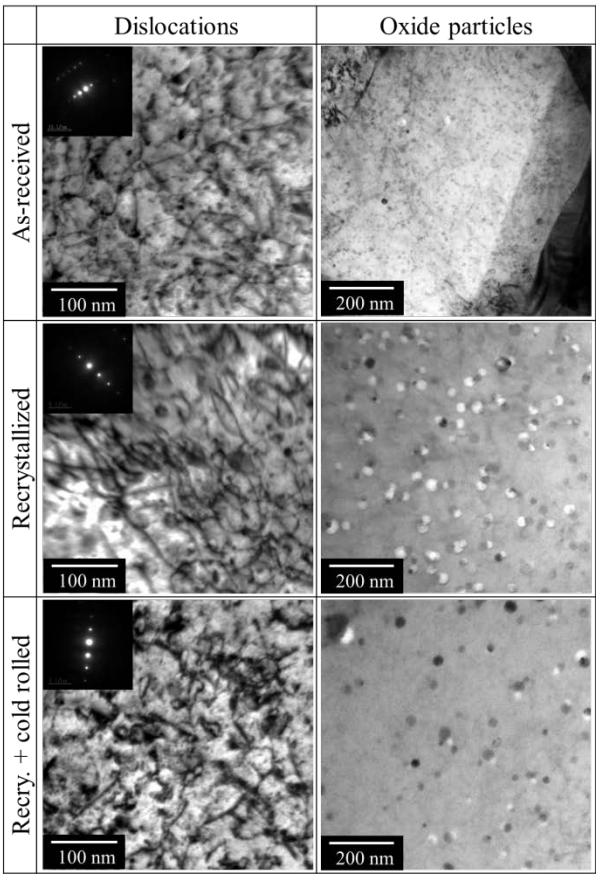

Fig. 4 More detailed TEM microstructures observed with a dislocation contrast (left) and void contrast (right)

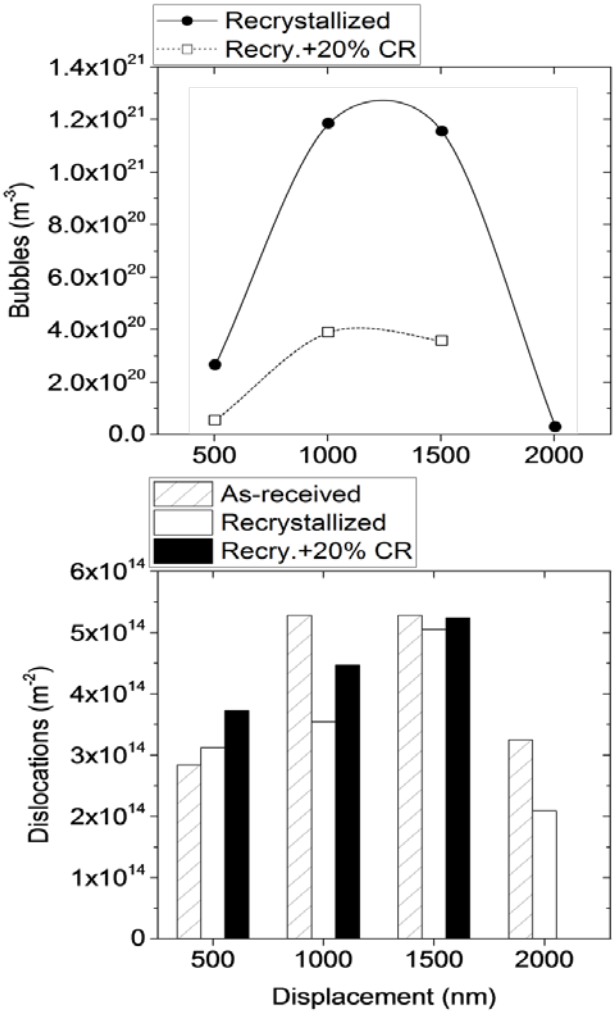

Fig. 5 The distribution profiles of dislocation with <200> g vector (bottom) and bubble number density (top) after dual-ion irradiation

Table 3 The estimated irradiation hardening and experimentally measured hardening at 250 nm of indentation depth.

	hardening of dislocation, ΔH_D			hardening of bubbles, ΔH_B		Total	Experiment
	$\alpha_{line\ type}$ =0.212	$\alpha_{loop\ type}$ =0.65	ΔH_D	α	ΔH_B	$\Delta H=\Delta H_{D\text{-}Line}+\Delta H_{D\text{-}Loop}+\Delta H_B$	@ 250nm
1) As-received	347	266	613	α=0	0	613	811
				α=0.1	0	613	
				α=0.2	0	613	
2) Recrystallized	1,048	56	1,104	α=0	0	1,104	1,079
				α=0.1	120	1,224	
				α=0.2	240	1,344	
3) Cold rolled	218	223	441	α=0	0	441	447
				α=0.1	67	508	
				α=0.2	133	574	